Constraints on the cosmological relativistic energy density

Andrew R. Zentner[1,*] and Terry P. Walker[1,2,†]

[1]*Department of Physics, The Ohio State University, Columbus, OH 43210, USA*
[2]*Department of Astronomy, The Ohio State University, Columbus, OH 43210, USA*

(Dated: December 17, 2001)

We discuss bounds on the cosmological relativistic energy density as a function of redshift, reviewing the big bang nucleosynthesis and cosmic microwave background bounds, updating bounds from large scale structure, and introducing a new bound from the magnitude-redshift relation for Type Ia supernovae. We conclude that the standard and well-motivated assumption that relativistic energy is negligible during recent epochs is not necessitated by extant data. We then demonstrate the utility of these bounds by constraining the mass and lifetime of a hypothetical massive big bang relic particle.

PACS numbers: 98.80.-k, 98.70.Vc

arXiv:astro-ph/0110533v2 3 Jan 2002

I. INTRODUCTION

Cosmological constraints on the relativistic energy density (RED) of the Universe, particularly the bound derived from the successful prediction of the primordial abundances of D, ^{4}He, and ^{7}Li, provide perhaps the strongest connections between cosmology and particle physics. In this paper we examine constraints on the RED (To be specific, we consider constraints on the energy density of any particle that obeys an equation of state $P = \rho/3$.) at various cosmological epochs and discuss how these bounds can be used to limit the mass and lifetime of an unstable big bang relic particle. We review the classic big bang nucleosynthesis (BBN) bound and the bound from the cosmic microwave background (CMB) anisotropy power spectrum. We present a new bound derived from the magnitude-redshift relation of Type Ia supernovae (SNIa), and we update the bound from large scale structure (LSS). Although we will attempt to derive bounds that are independent of additional cosmological parameters, where necessary we will borrow constraints from other techniques in order to further limit the relativistic energy density of the Universe. For example, when needed we adopt the bound $0.1 \leq \Omega_{\rm M} \leq 0.5$ ($\Omega_{\rm M}$ is the matter density relative to the critical density today, $\rho_{\rm crit} \equiv 3H_0^2/8\pi G$), consistent with recent measurements of the contemporary matter density from lensing [1], the rich cluster baryon fraction [2], mass-to-light ratio estimates [3], and the power spectrum of the Lyα forest [4]. We also adopt a hard limit on the Hubble parameter ($h \equiv H_0/100$ kms^{-1}Mpc^{-1}) of $0.56 \leq h \leq 0.88$ in accordance with the 2σ range of the HST Key Project [5].

*Electronic address: zentner@pacific.mps.ohio-state.edu
†Electronic address: twalker@pacific.mps.ohio-state.edu

II. CONSTRAINTS ON RELATIVISTIC ENERGY

A. Nucleosynthesis Constraint

It has long been known that an increase in the RED of the Universe during BBN leads to an overproduction of ^{4}He [6] (BBN reviews include [7]). Prior to freeze-out of the weak interactions, the neutron-to-proton ratio (n/p) tracks its equilibrium value. As the Universe expands and cools, the weak interactions freeze-out and (n/p) freezes in. Freeze-out occurs when the weak interaction rates become comparable to the expansion rate H, given by $H^2 = 8\pi G\rho/3$, where ρ is the mean cosmological energy density. Once deuterium can be synthesized nearly all available neutrons are incorporated into ^{4}He. Increasing the energy density of the Universe during BBN increases the expansion rate, causing the weak interactions to freeze-out at a higher temperature and therefore, at a higher value of (n/p). An increased expansion rate also allows less time for free neutron decay. Both effects make more neutrons available for ^{4}He synthesis.

In addition, BBN production of ^{4}He slowly increases with the baryon density or equivalently, the baryon-to-photon ratio, $\eta \equiv n_B/n_\gamma$. Since BBN production of deuterium is a rapidly decreasing function of η, the baryon density can be deduced from the D/H ratio observed in QSO absorption line systems. Furthermore, because ^{4}He has been produced in stars since BBN, the observed ^{4}He abundance places an upper limit on its primordial abundance. Armed with this upper bound to primordial ^{4}He and an independent measure of η, we can place a bound on the RED during the BBN epoch ($z \sim 10^9$).

We illustrate the current status of the BBN bound to the RED as follows (see the recent analyses of [8] for details). We adopt a liberal range for the primordial D/H ratio that accommodates recent observations of deuterium in several QSO absorption line systems [9]: $1.75 \leq 10^5$(D/H) ≤ 5.0. We then bound the RED by taking a conservative bound on the ^{4}He mass fraction, $Y_P \leq 0.25$. This bound is consistent with both the low

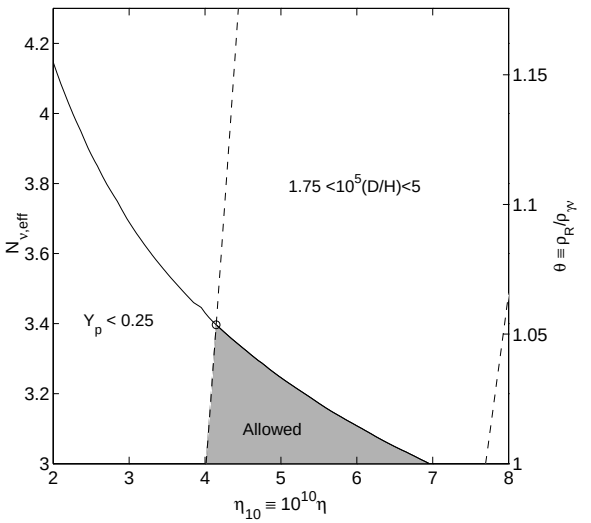

FIG. 1: The BBN bound on the RED. The region bounded by the dashed curves delimits the parameter space for which the theoretically predicted and observed values of D/H are consistent. Likewise, the data on Y_P are consistent with predictions in the region below the solid curve. The intersection, marked by the circle, shows the maximum value of $N_{\nu,eff}$ that can be made consistent with these limits on Y_P and D/H.

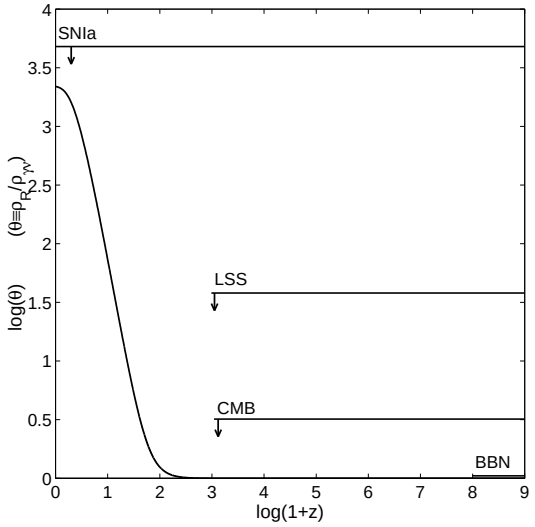

FIG. 2: Constraints on the RED. The horizontal lines denote the maximum value of $\theta(z)$ allowed by BBN, CMB, LSS and SNIa. Notice that the BBN constraint in the lower right-hand corner is hardly noticeable (*i.e.*, very strict). By extending the limits to higher redshift, we have made the assumption that after BBN relativistic energy is only injected and never removed. The curved line shows $\theta(z)$ in a scenario where a massive big bang relic with $M_{keV}Y = 1.2 \times 10^{-3}$ decays with lifetime $\tau_{yr} = 2 \times 10^9$. There are additional CMB and LSS constraints on relativistic energy injected after $z \sim 1000$; however, they do not rule out the decay shown above (see sections III and IV).

[10] and high [11] zero-metallicity extrapolations of low-metallicity HII region data (but see [12]). We follow convention by expressing limits on relativistic energy in terms of the energy carried by an effective number of light neutrino species, $N_{\nu,eff}$. The RED at some redshift z, after e^+e^- annihilation, is related to $N_{\nu,eff}$ by

$$\theta(z) \equiv \frac{\rho_{\rm R}(z)}{\rho_{\gamma\nu}(z)} = [1 + 0.135(N_{\nu,eff} - 3)], \qquad (1)$$

where we scale the RED by $\rho_{\gamma\nu}(z)$ which is the standard model RED carried by photons and three massless neutrino species (with a current CMB temperature of 2.725 K [13], $\Omega_{\gamma\nu} \equiv \rho_{\gamma\nu}(z=0)/\rho_{\rm crit} = 4.18h^{-2} \times 10^{-5}$). In Figure 1, we show regions of the η-$N_{\nu,eff}$ plane allowed by the observed ^{4}He and D abundances. The data require that $N_{\nu,eff} \lesssim 3.4$ or, in terms of the RED during nucleosynthesis $\theta_{\rm BBN} \equiv \theta(z = 10^9)$,

$$\theta_{\rm BBN} \lesssim 1.05. \qquad (2)$$

In Figure 2, we show the amount of extra relativistic energy permitted during BBN.

There are two important caveats regarding the BBN RED bound. First, although (2) is a rather stringent bound on the RED, corresponding to an increase of $\sim 5\%$ over the standard $\rho_{\gamma\nu}$, it only applies during the epoch of nucleosynthesis. Relativistic energy injected after BBN is not subject to this bound (in Section III, we discuss a toy model in which relativistic energy is injected into the Universe after the light nuclide abundances have been fixed). Second, the BBN RED bound is flavor dependent in the sense that extra relativistic energy in the form of degenerate electron neutrinos changes the rates of the weak interactions that inter-convert protons and neutrons thereby changing theoretical BBN yields. Introducing an appropriate amount of electron neutrino degeneracy can always compensate for excess relativistic energy present during nucleosynthesis [14, 15], nullifying the BBN RED constraint.

B. CMB Constraint

The CMB anisotropy power spectrum is also sensitive to the RED of the Universe at recombination, primarily through the early Integrated Sachs-Wolfe (ISW) effect. The erosion of gravitational potentials due to incomplete matter domination at recombination leads to a boost in power, particularly near the first acoustic peak (for a review see [16]). CMB constraints on relativistic energy complement those from BBN in two ways. First, the CMB constraints are flavor independent; the power spectrum measures relativistic energy regardless of its form. Second, the CMB constrains the RED at later epochs so that the CMB can be used to study the injection of relativistic energy after the epoch of nucleosynthesis, for example, by massive neutrino decays.

Wang, Tegmark & Zaldarriaga [17] have compiled a combined CMB data set including the recent results from

the BOOMERANG [18], MAXIMA [19] and DASI [20] experiments. Hannestad [21] has performed a likelihood analysis on this combined data set and found, with weak priors on the Hubble and tilt parameters and the baryon density, $N_{\nu,eff} \leq 19$ with 95% confidence. In terms of the RED present at recombination, $\theta_{\rm CMB} \equiv \theta(z \approx 1100)$, this bound is

$$\theta_{\rm CMB} \lesssim 3.2 \tag{3}$$

as depicted in Figure 2.

A cautionary note is in order. Although the priors chosen by Hannestad are quite conservative, it must be borne in mind that the bound in (3) does depend upon these priors. For example, by adopting tighter, yet reasonable, prior constraints on h and η, Hannestad shrinks the above limit to $N_{\nu,eff} \leq 17.5$ at 95% confidence [21] (see also [22]). Kneller *et al.*, [15] have explored the prior dependence of these bounds in detail, showing that the bound on $N_{\nu,eff}$ scales with the upper bound chosen for $\Omega_{\rm M}$ (*i.e.*, interesting CMB bounds on the RED require a prior constraint on $\Omega_{\rm M}$).

C. Constraints from Type Ia Supernovae

Given a distant population of so-called "standard candles", the magnitude-redshift relation is a powerful way to determine cosmological parameters directly [23]. In a standard FRW cosmology, the apparent bolometric magnitude, $m(z)$, of a standard candle is related to its absolute bolometric magnitude, M, and redshift by

$$m(z) = M + 5\log(\mathcal{D}_L(z, \Omega_{\rm M}, \Omega_\Lambda, \Omega_{\rm R})) - 5\log(H_0) + 25, \tag{4}$$

where H_0 is the Hubble parameter in $\rm kms^{-1}Mpc^{-1}$. $\mathcal{D}_L$ is the "Hubble-constant-free" luminosity distance in Mpc, given by

$$\mathcal{D}_L = c(1+z)\sqrt{\frac{1}{|\Omega_{\rm k}|}}\Sigma\left(\sqrt{|\Omega_{\rm k}|}\int_0^z \frac{d\overline{z}}{\sqrt{(1+\overline{z})^2(1+\Omega_{\rm M}\overline{z}) + (1+\overline{z})^2(2+\overline{z})\overline{z}\Omega_{\rm R} - \overline{z}(2+\overline{z})\Omega_\Lambda}}\right)$$

where c is in $\rm kms^{-1}$, $\Omega_{\rm k} \equiv 1 - \Omega_{\rm M} - \Omega_\Lambda - \Omega_{\rm R}$, and

$$\begin{aligned}\Sigma(x) &= \sin(x) \quad \text{if} \quad \Omega_{\rm k} < 0 \\ &= x \quad \text{if} \quad \Omega_{\rm k} = 0 \\ &= \sinh(x) \quad \text{if} \quad \Omega_{\rm k} > 0.\end{aligned}$$

The matter, radiation and cosmological constant energy densities enter $\mathcal{D}_L$ with different powers of z, making it possible to utilize observations of standard candles over a range of redshifts to determine the cosmological density parameters (for a review, see [24]).

Two groups, the Supernova Cosmology Project [25] and the High-z Supernova Search Team [26], have been engaged in a systematic study of the magnitude-redshift relation of high-redshift, type Ia supernovae in an effort to constrain $\Omega_{\rm M}$ and Ω_Λ. We have re-analyzed the data of Perlmutter et al. [25] allowing for a non-negligible contribution from $\Omega_{\rm R}$. For simplicity, we have assumed flatness to be a robust result of CMB measurements [27] and have performed a maximum-likelihood analysis (we take $\mathcal{L} \propto e^{-\chi^2/2}$ subject to the priors $\Omega_{\rm M} \geq 0$, $\Omega_{\rm R} \geq 0$) in order to derive constraints on $\Omega_{\rm M}$ and $\Omega_{\rm R}$ with $\Omega_\Lambda \equiv 1 - \Omega_{\rm M} - \Omega_{\rm R}$[1].

In Figure 3, we show the constraints on $\Omega_{\rm M}$ and $\Omega_{\rm R}$ from SNIa. The projection $\Omega_{\rm R} = 0$ is consistent with earlier analyses that found $\Omega_{\rm M} \sim 0.3$ and $\Omega_\Lambda \sim 0.7$ assuming the RED to be negligible. Allowing for relativistic energy density, we find a degenerate set of $\Omega_{\rm M}$ and $\Omega_{\rm R}$ that are consistent with the SNIa data: the high-matter-content (*i.e.*, 30% matter, 70% cosmological constant) flat Universe and the high-radiation-content (*i.e.*, 20% radiation, 80% cosmological constant) flat Universe are equally good fits. Observe that regardless of whether relativistic energy is allowed or not, the SNIa data require a large cosmological constant ($0.6 \lesssim \Omega_\Lambda \lesssim 0.9$).

The 95% confidence contour is approximately fit by the region

$$\Omega_{\rm R} + 0.62\Omega_{\rm M} \approx 0.17 \pm 0.08. \tag{5}$$

It is not surprising that the data pick out this degenerate valley in the $\Omega_{\rm M}$-$\Omega_{\rm R}$ plane because most of the SNIa data are from $z \sim 0.5$ and our degenerate valley represents the parameters with approximately constant luminosity distance at this redshift. The degeneracy can be further understood with the help of Figures 3 & 4. Dashed and

[1] Relaxing flatness yields a less restrictive bound on $\Omega_{\rm R}$ but much of the favored region of parameter space would be ruled out by age considerations, CMB measurements, or the aforementioned bounds on $\Omega_{\rm M}$.

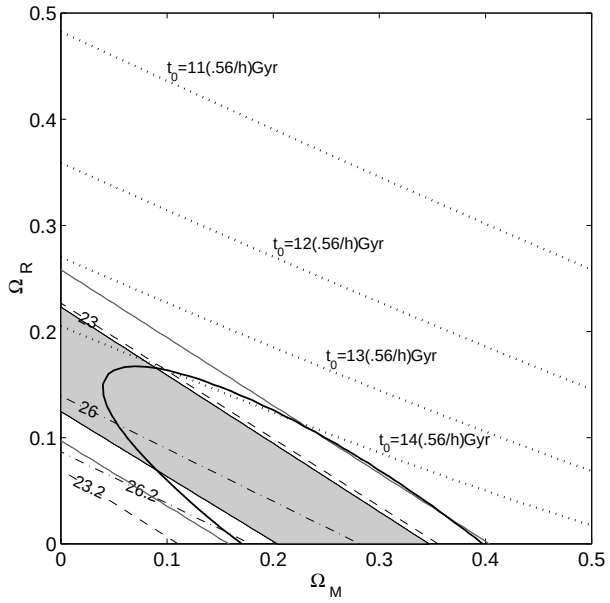

FIG. 3: 68% (filled) and 95% (open) confidence contours in the $\Omega_{\rm M}$-$\Omega_{\rm R}$ plane. For illustration, we show several labeled isochrones (dotted) and the elliptical 95% confidence contour obtained by adding an additional prior constraint of $\Omega_{\rm M} = 0.3 \pm 0.1$ (solid, heavy). Also shown are contours of constant effective m_B for SNIa at redshifts of $z = 0.5$ (dashed at $m_B = 23,\ 23.2$) and $z = 1.5$ (dash-dot at $m_B = 26,\ 26.2$).

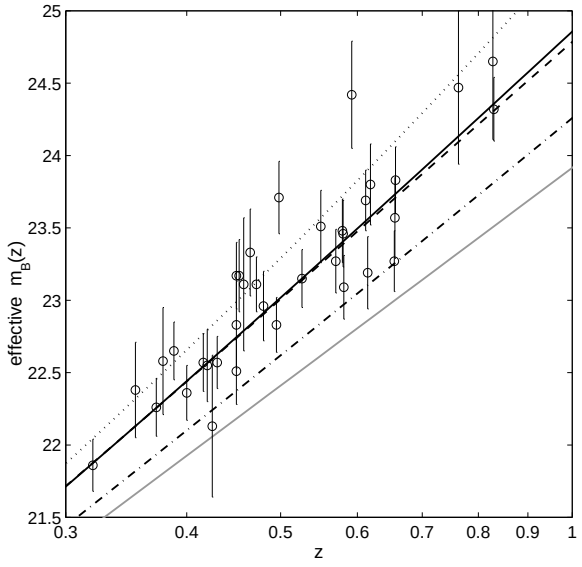

FIG. 4: The high-redshift portion of the Hubble diagram for the SCP data (with 1σ error bars) alongside the magnitude-redshift relation in several flat cosmologies: $\Omega_{\rm M} = 0.3$ and $\Omega_{\rm R} = 0$ (heavy, solid), $\Omega_{\rm M} = 0$ and $\Omega_{\rm R} = 0.2$ (dashed), $\Omega_\Lambda = 1$ (dotted), $\Omega_{\rm M} = 1$ (dash-dot), $\Omega_{\rm R} = 1$ (light, solid).

dot-dashed lines in Figure 3 depict contours of constant apparent magnitude at redshifts $z = 0.5$ and $z = 1.5$ respectively. As most of the SNIa data lie near $z \sim 0.5$, the confidence region is nearly parallel to lines of constant m_B at $z = 0.5$. At higher redshifts, lines of constant apparent magnitude have a more shallow slope and are closer together, thus observations of SNIa at $z > 0.5$ can break the matter-radiation degeneracy.

Figure 4 further illustrates the large lever arm of high-z SNIa for cosmological parameter estimation. Notice that the magnitude-redshift relation in a high-matter-content Universe ($\Omega_{\rm M} = 0.3$, $\Omega_{\rm R} = 0$) is quite similar to that in a high-radiation-content Universe ($\Omega_{\rm R} = 0.2$, $\Omega_{\rm M} = 0$) at $z \lesssim 0.5$. At higher redshift, one begins to probe the epoch prior to matter-Λ and/or radiation-Λ equality; the cosmological constant becomes increasingly unimportant compared to radiation and/or matter and the two curves begin to diverge. The SCP data only extend to $z = 0.83$, therefore they cannot be used to scrutinize this earlier phase and they cannot distinguish between a high-matter-content Universe and a high-radiation-content Universe. The proposed Supernova Acceleration Probe ([http://snap.lbl.gov]) may have the ability to break this degeneracy by observing many more SNIa at significantly higher redshift.

Marginalizing over $\Omega_{\rm M}$ by integrating the likelihood, we obtain a bound on the RED at low redshift $\theta_{\rm SNIa} \equiv \theta(z \lesssim 0.5)$,

$$\theta_{\rm SNIa} \lesssim 3.4h^2 \times 10^3 \ (68\%) \text{ or } 4.8h^2 \times 10^3 \ (95\%). \quad (6)$$

In terms of the RED today, the bound is $\Omega_{\rm R} \leq 0.14$ (68%) and $\Omega_{\rm R} \leq 0.20$ (95%).

The SNIa constraint on the RED applies during recent epochs, namely, $z \lesssim 0.5$, as can be seen in Figure 2. Of course, in light of other estimates of cosmological parameters, the allowed region in Fig. 3 is not equally probable. Estimates of the contemporary matter density of the Universe favor the region $\Omega_{\rm M} = 0.3 \pm 0.1$ and would slightly reduce the SNIa upper bound on the RED. This is illustrated in Figure 3 where we also plot the 95% confidence contour obtained with the additional prior constraint $\Omega_{\rm M} = 0.3 \pm 0.1$. This prior constraint on the matter density reduces the 95% bound on $\Omega_{\rm R}$ by about 25%.

Note also that the SNIa bound on the contemporary RED is more stringent than bounds that follow from the requirement that the expansion age of the Universe be at least as large as the ages of the oldest objects in the Universe. In Figure 3, the *entire* region delineated by SNIa data corresponds to an acceptable age. In particular, a high-radiation-content Universe with $\Omega_{\rm M} = 0.04$, $\Omega_{\rm R} = 0.20$, $\Omega_\Lambda = 0.76$ and a Hubble parameter at the extreme lower limit, $h = 0.56$, is 13.8 Gyr old. Even with $h = 0.72$, $t_0 \simeq 10.7$ Gyr, a value that is not grossly inconsistent with the ages of the oldest stars and globular clusters [28].

D. Large Scale Structure Constraints

The effect of additional relativistic energy on the growth of large scale structure (LSS) has been studied by numerous authors [29, 30, 31, 32, 33]. Typically, the introduction of "hot dark matter" was considered a means to suppress power on small scales and thus reconcile an $\Omega_{\rm M} = 1$, Cold Dark Matter (CDM) cosmology with the observed power spectrum derived from galaxy surveys [34]. Conversely, too much relativistic energy adversely affects the growth of structure and therefore LSS can be used to constrain the RED. In light of mounting evidence, the CDM paradigm has given way to the so-called ΛCDM paradigm with $\Omega_{\rm M} \sim 0.3$ and $\Omega_\Lambda \sim 0.7$. With this in mind, we revise previous work in order to constrain the relativistic energy content of the Universe using LSS.

The most striking feature of a CDM or ΛCDM type power spectrum is a break in the power law at, roughly speaking, the co-moving horizon scale at matter-radiation equality

$$\lambda_{\rm EQ} \simeq 16(\Omega_{\rm M}h)^{-1}\ h^{-1}\ {\rm Mpc}. \tag{7}$$

This feature arises because the growth of sub-horizon sized perturbations is quelled by the cosmological expansion during radiation domination. Hence, perturbations on scales smaller than $\lambda_{\rm EQ}$ are suppressed by a factor $\sim (\lambda/\lambda_{\rm EQ})^2$ relative to scales that were super-horizon sized at matter radiation equality.

If the RED of the Universe is contained entirely in photons and three light neutrino species, and if the primordial power spectrum is nearly scale-invariant, the ΛCDM matter power spectrum can be expressed in terms of only one quantity, the shape parameter $\Gamma \simeq \Omega_{\rm M}h$ [35] (this neglects the effect of baryons, see [36]). Several authors have used LSS observations on linear scales to infer acceptable values of the shape parameter [37]. One of the more permissive of these determinations is the 95% range

$$0.06 \leq \Gamma \leq 0.46, \tag{8}$$

quoted by Efstathiou & Moody [38], which we will use to constrain the RED.

In the presence of excess relativistic energy, the horizon scale at matter-radiation equality is no longer given by (7). Rather,

$$\lambda_{\rm EQ} \simeq 16(\Omega_{\rm M}h)^{-1}\sqrt{\Omega_{\rm R}/\Omega_{\gamma\nu}}h^{-1}\ {\rm Mpc} \tag{9}$$

and the effective shape parameter is therefore given by [31]

$$\Gamma \simeq \Omega_{\rm M}h\theta^{-1/2}. \tag{10}$$

Taking the lower bound $\Gamma > 0.06$ we immediately come upon a generic constraint on the mean RED:

$$\theta \leq \left(\frac{\Omega_{\rm M}h}{0.06}\right)^2. \tag{11}$$

With our conservative assumptions that $\Omega_{\rm M} \leq 0.5$ and $h \leq 0.88$, the corresponding restriction on the RED during (and prior to) the epoch of matter-radiation equality, $\theta_{\rm LSS} \equiv \theta(z = z_{\rm EQ})$, is

$$\theta_{\rm LSS} \lesssim 54 \tag{12}$$

where $1 + z_{\rm EQ} \equiv \Omega_{\rm M}/\Omega_{\rm R}$. The relative weakness of this bound is due to our conservative lower bound on Γ. Taking the 95% band of Eisenstein & Zaldarriagga [37], $0.15 \leq \Gamma \leq 0.58$, results in $\theta_{\rm LSS} \lesssim 9$.

Note that this constraint (12) allows the epoch of matter-radiation equality to be at redshifts as low as $z_{\rm EQ} \approx 120$. We can obtain a more stringent bound on the RED by following an argument invoked by Turner, Steigman & Krauss [29], Steigman & Turner [30] and Turner & White [33]. Assuming a nearly scale-invariant primordial power spectrum, data from the COBE DMR experiment [39] indicate that the rms density contrast at horizon crossing is on the order of $\delta_{\rm H} \sim$ few $\times\ 10^{-5}$ [40]. Meanwhile, measurements of the galaxy correlation function reveal nonlinear clustering on scales smaller than a critical scale, $\lambda_{\rm NL} \sim 5h^{-1}$ Mpc [41]. We adopt the conservative constraint that perturbations on scales smaller than $\lambda_{\rm NL}$ must have grown by at least a factor of $\gamma_{\rm min} \equiv 10^3$ in order for the rms perturbation on these scales to be nonlinear. In linear perturbation theory, density fluctuations grow as $\delta \propto (1+z)^{-1}$ during matter domination and only logarithmically during radiation domination. This implies that the matter dominated epoch must span at least three orders of magnitude in redshift. With $\Omega_{\rm M} \leq 0.5$ this, in turn, imposes the limitation

$$\theta_{\rm LSS}h^2 \lesssim 12 \text{ or } \theta_{\rm LSS} \lesssim 38, \tag{13}$$

where we have taken $h \geq 0.56$. This constraint is shown in Figure 2 where we summarize the constraints on relativistic energy imposed by BBN, the CMB, LSS and the SNIa magnitude-redshift relation.

III. CONSTRAINING RELIC DECAYS

In the preceding section we reported limits on the RED at various epochs. In the absence of electron neutrino degeneracy, the BBN constraint on the RED is, by far, the most stringent; it leaves little room for any non-standard relativistic energy during the BBN epoch. One way to

circumvent the BBN constraint is to inject relativistic energy after nucleosynthesis has ended, for instance, by the decay of a particle that was non-relativistic during BBN ($M \gg 1$ MeV) into relativistic products. As such, the study of relic particle decays comes part and parcel with constraints on relativistic energy. We examine the simple case of a massive, unstable big bang relic which may be pertinent to physics "beyond the Standard Model" and discuss constraints on the relic's mass and lifetime that follow from the bounds on the RED in Section II. It is important to note that, aside from the CMB constraint, the assumption that the relic is very massive is not critical. In general, the particle must be non-relativistic at decay in order for its decay product's energy density to be comparable to or greater than $\rho_{\gamma\nu}$.

Consider the decay of a massive relic particle X, with lifetime τ, into relativistic products. Had X not decayed, the energy density in these particles today would be

$$\Omega_{\rm X} h^2 \simeq 274 M_{keV} Y. \tag{14}$$

In (14), M_{keV} is the mass of the particle in keV and Y is the ratio of the number density of the particle to the entropy density ($Y \simeq 0.039$ for a light neutrino, $Y \simeq 2\times10^{-10}$ for a 5 GeV, Dirac neutrino). Given a specific particle physics model in which X is produced in the early Universe, Y is fixed (in the absence of subsequent entropy production); however, in order to make the constraints on heavy particle decays as generic as possible, we have chosen to keep Y as an explicit, free parameter. Further, we assume that the daughter particles are weakly-interacting (constraints on radiative decays are quite severe [42]). In all analytic calculations we assume that decays occur simultaneously at $t = \tau$. Energy conservation during decay demands that the present energy density in decay products be $\Omega_{\rm D} = \Omega_{\rm X}/(1+z_{\rm D})$, where $z_{\rm D}$ is the redshift at decay (*i.e.*, z at $t = \tau$). Assuming the Universe to be X-dominated prior to decay,

$$\Omega_{\rm D} h^2 \simeq 5.1\times10^{-4} M_{keV}^{4/3} Y^{4/3} \tau_{yr}^{2/3} \tag{15}$$

where τ_{yr} is the lifetime of X in years.

A. CMB Constraints on Relic Properties

One constraint on relic properties follows from the requirement that the total energy density in relativistic particles $\Omega_{\rm R} = \Omega_{\gamma\nu} + \Omega_{\rm D}$, fall under the CMB bound in (3) during the epoch of recombination. If the particle decays prior to recombination the CMB constraint (3), along with the analytic approximation of (15), implies that[2]

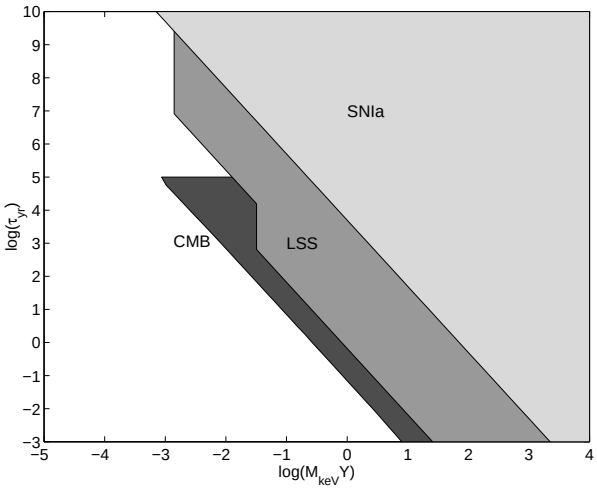

FIG. 5: The regions of parameter space for a massive relic decay that are excluded by CMB (heavily shaded), LSS (moderately shaded) and SNIa (lightly shaded) arguments. Each excluded region extends to arbitrarily high $M_{keV}Y$.

$$M_{keV}^2 Y^2 \tau_{yr} \lesssim 7.5\times10^{-2}. \tag{16}$$

For pertinent lifetimes, $10^{-3} \lesssim \tau_{yr} \lesssim 10^5$, the excluded region of parameter space is displayed in Figure 5.

Post-recombination X decays modify the CMB power spectrum through the ISW effect and through shifts in the multipole positions of the acoustic peaks due to a change in the angular diameter distance to the surface of last-scattering. It is possible to use this modification of the observed CMB anisotropy power spectrum to constrain post-recombination X decays [43], but these constraints would not be generic because the gravitational dynamics of the relic as well as its decay scheme can contribute to the ISW effect. Such constraints would have to be developed on a case-by-case basis considering the relic mass and relic abundance separately; however, we mention a specific case that evades the CMB bound and contributes a significant RED at the present epoch in section IV. In the following subsection, we show that the growth of LSS can place severe, yet generic, constraints on post-recombination decays.

B. LSS Constraints on Relic Decays

Large scale structure considerations also lead to bounds on decaying relics. Utilizing (15), θ can be ex-

[2] The CMB constraint on relativistic energy is strict enough that the assumption of X-domination prior to decay is untenable, making it necessary to integrate the equations governing heavy WIMP decay in a flat, Friedmann cosmology. We have performed the necessary integration and find that the above analytic bound is typically accurate to within 20%.

pressed as $\theta \simeq 1+12.2M_{keV}^{4/3}Y^{4/3}\tau_{yr}^{2/3}$. Consequently, the effective shape parameter (10) may be written

$$\Gamma \simeq \Omega_{\rm M} h[1+12.2M_{keV}^{4/3}Y^{4/3}\tau_{yr}^{2/3}]^{-1/2} \tag{17}$$

from which we conclude that

$$M_{keV}^2 Y^2 \tau_{yr} \simeq 188[(\Omega_{\rm M}h)^2-\Gamma^2]^{3/2}. \tag{18}$$

Again, taking $\Omega_{\rm M} \leq 0.5$, $h \leq 0.88$ and $\Gamma \geq 0.06$, we deduce that

$$M_{keV}^2 Y^2 \tau_{yr} \lesssim 16. \tag{19}$$

Observe that (19) restricts the combination $M_{keV}^2 Y^2 \tau_{yr}$. As has been underscored by McNally & Peacock and Bharadwaj & Sethi [32], the power spectrum will also exhibit a feature on small scales corresponding to the transition between radiation domination and an early matter dominated (domination by X particles) phase. As the co-moving horizon scale during the first epoch of matter-radiation equality is given by

$$\lambda_{\rm X} \simeq \frac{1}{17.1 M_{keV} Y}\ {\rm Mpc}, \tag{20}$$

this small-scale feature can, in principle, constrain the combination $M_{keV}Y$ alone. In practice, however, much of the interesting region of relic parameter space would correspond to nonlinear scales and such a constraint would require a better theoretical handle on nonlinear clustering and bias.

We can strengthen the bound in (19) by requiring that structure grow sufficiently. As Steigman and Turner [30] have noted, there are two ways in which this can occur. One way was mentioned in Section II D, namely, that the relic decay early enough so that the most recent epoch of matter domination began at a redshift $(1+z_{\rm EQ}) \geq 10^3$. The redshift of equality is $(1+z_{\rm EQ}) \simeq \Omega_{\rm M}/\Omega_{\rm D}$ and using (14) and (15) we find that this scenario requires

$$M_{keV}^2 Y^2 \tau_{yr} \lesssim 0.66 \tag{21}$$

and is relevant for lifetimes in the range $10^{-3} \lesssim \tau_{yr} \lesssim 10^5$.

In the presence of a massive unstable relic however, there can be two phases of matter domination, an early X dominated phase and a second matter dominated phase after relic decay. It may be possible for perturbations on scales $\lambda < \lambda_{\rm NL}$ to take advantage of both of these periods of growth and thereby grow by a factor greater than $\gamma_{\rm min}$. X domination begins at redshift $(1+z_{\rm X}) = \Omega_{\rm X}/\Omega_{\gamma\nu}$, followed by decay at redshift $(1+z_{\rm D}) = \Omega_{\rm X}/\Omega_{\rm D}$. Thus the total growth factor for scales *smaller* than the horizon scale at X domination, $\lambda_{\rm X}$, is

$$\gamma \simeq \frac{(1+z_{\rm X})}{(1+z_{\rm D})}(1+z_{\rm EQ}) \simeq 2.4\times 10^4 \Omega_{\rm M} h^2. \tag{22}$$

With our aforementioned limits on $\Omega_{\rm M}$ and h, these scales grow by a maximum of $\gamma \simeq 9.3\times 10^3$. Perturbations that enter the horizon after X domination begins, grow by a smaller factor:

$$\gamma(\lambda > \lambda_{\rm X}) \simeq 9.3\times 10^3 \left(\frac{\lambda_{\rm X}}{\lambda}\right)^2. \tag{23}$$

Compelling $\gamma(\lambda_{\rm NL})$ to be greater than $\gamma_{\rm min}$ forces

$$M_{keV} Y \lesssim 3.6h\times 10^{-2} \lesssim 3.2\times 10^{-2}. \tag{24}$$

Combining (19), (21) and (24), we summarize the LSS constraints on early relic decays as

$$\begin{aligned} &M_{keV}^2 Y^2 \tau_{yr} \lesssim 0.66 \quad \text{or} \\ &M_{keV}^2 Y^2 \tau_{yr} \lesssim 16 \quad \text{and} \quad M_{keV} Y \lesssim 3.2\times 10^{-2}. \end{aligned} \tag{25}$$

The excluded region is shown in Figure 5.

The above constraints (25) are pertinent for lifetimes in the range $10^{-3} \lesssim \tau_{yr} \lesssim 10^6$ because we assumed that the turnover in the power spectrum is indicative of $\lambda_{\rm EQ}$, the horizon scale at the epoch of matter-radiation equality *after* X decay. Alternatively, the X particles may have very large lifetimes, $\tau_{yr} \gg 10^6$, in which case the turnover in the power spectrum would be indicative of $\lambda_{\rm X}$, the horizon scale at the first epoch of matter-radiation equality, *prior to* X decay. In this case, the effective shape parameter is simply

$$\Gamma \simeq (\Omega_{\rm X}+\Omega_{\rm M})h. \tag{26}$$

If we adopt our limiting case that $\Omega_{\rm M} \geq 0.1$ in order to be consistent with various measures of the contemporary matter density, we find that the restriction $\Gamma \leq 0.46$ from (8) asserts that

$$M_{keV} Y \lesssim 1.2\times 10^{-3}. \tag{27}$$

We illustrate this bound in Figure 5 by the vertical boundary for $\tau_{yr} \gtrsim 10^7$. Lastly, because $(1+z_{\rm EQ}) \sim 10^4$ in this scenario and $\Omega_{\rm X}$ is not more than a factor of five larger than our lower bound on $\Omega_{\rm M}$, requiring $\gamma_{min} \gtrsim 10^3$ provides only a weak restriction on X lifetimes. It may be more useful to take advantage of the large scale feature that would be present in the power spectrum due to the injection of relativistic energy in order to limit relic properties. We do not explore such bounds as this would require specifying M_{keV} and Y separately.

C. SNIa Constraint on Relic Decays

With the SNIa bound on relativistic energy from Section II C, it is now easy to obtain a SNIa bound on the relic decay properties. Using (15) and the 95% upper limit in (6), we have

$$M_{keV}^2 Y^2 \tau_{yr} \lesssim 5.3 \times 10^3, \tag{28}$$

where we have once again assumed $h \leq 0.88$. Notice that this follows from a bound on the contemporary RED and, therefore, is most pertinent to late decays (*i.e.*, $\tau_{yr} \gtrsim 10^8$). Again, this constraint is shown in Figure 5 where our bounds on the properties of decaying relics are summarized.

IV. CONCLUSIONS

Constraints on the cosmological RED can provide a fundamental probe of particle physics beyond the standard model. In this paper we have discussed constraints on the RED during four distinct epochs arising from BBN, the CMB, LSS and SNIa (see Figure 2). Further, we have shown how these bounds constrain the mass and lifetime of a hypothetical big bang relic (see Figure 5). Somewhat surprisingly, the RED at the current epoch is relatively unconstrained: we have shown that the magnitude-redshift relation for SNIa is consistent with a flat universe comprised of up to 20% relativistic energy. Conventional wisdom suggests that the RED today must be small to allow for sufficient growth of large scale structure and not appreciably alter the CMB anisotropy power spectrum. The LSS bound does, in fact, significantly limit the RED *near the epoch of matter-radiation equality*. Any RED consistent with subsequent growth of LSS, redshifted to the current epoch, would be quite small. Conversely, a RED that is large yet acceptable with respect to the SNIa bound would clearly inhibit the growth of LSS if it were redshifted to the past. However, a long-lived particle that decays sufficiently late as to avoid the LSS constraint could nevertheless contribute substantially to the RED today. In this case, the relevant constraint would be the aforementioned CMB bound (see Section III A). Avoiding the CMB constraint requires the X particles to be very long-lived if they are to contribute appreciably to the RED today. Consider a big bang relic with $M_{keV}Y = 1.2 \times 10^{-3}$(a 30 eV neutrino is an example of a particle with the necessary abundance) and a very long lifetime, $\tau_{yr} = 2 \times 10^9$. The decay products of this relic contribute $\Omega_{\rm D} h^2 \sim 0.1$ and its properties are marginally consistent with the growth of LSS . In addition, the decay products are produced sufficiently late so as to contribute an unconstrained ISW perturbation at low multipole moments, peaking around $\ell \sim 10$, and to change the angular diameter distance to the last-scattering surface by only $\sim 7\%$ (see Figures 3 and 4 of Kaplinghat *et al.*, [43]). These effects cannot be ruled out by current CMB data. In Figure 2 we show the evolution of the RED including the decay products of this hypothetical, long-lived big bang relic.

Acknowledgments

We would like to thank Jim Kneller, Savvas Koushiappas, Bob Scherrer, and Gary Steigman for many insightful comments and helpful discussions. We also wish to thank Rich Schugart and Jason Farris who performed some initial SNIa calculations as part of the NSF REU program at OSU. We acknowledge DOE contract DE-FG02-91ER40690 for support.

[1] L. Van Waerbeke, et al., Astron. and Astrophys. **358**, 30 (2000); D. M. Wittman, et al., Nature **405**, 143 (2000); L. Van Waerbeke, et al. (2001), astro-ph/0101511.
[2] B. Mathiesen, A. Evrard, and J. J. Mohr, Astrophys. J. Lett. **520**, L1 (1999); L. Grego, et al., Astrophys. J. **552**, 2 (2001).
[3] N. A. Bahcall, R. Cen, R. Davé, J. P. Ostriker, and Q. Yu, Astrophys. J. **541**, 1 (2000).
[4] R. A. C. Croft, D. H. Weinberg, M. Pettini, L. Hernquist, and N. Katz, Astrophys. J. **520**, 1 (1999); D. H. Weinberg, R. A. C. Croft, L. Hernquist, N. Katz, and M. Pettini, Astrophys. J. **522**, 563 (1999).
[5] W. L. Freedman, et al., Astrophys. J. **553**, 47 (2001).
[6] G. Steigman, D. N. Schramm, and J. Gunn, Phys. Lett. **B66**, 202 (1977).
[7] K. A. Olive, Nucl. Phys. Proc. Suppl. **80**, 79 (2000); K. A. Olive, G. Steigman, and T. P. Walker, Phys. Rept. **333**, 389 (2000).
[8] S. Burles, K. M. Nollett, J. W. Truran, and M. S. Turner, Phys. Rev. Lett. **82**, 4176 (1999); E. Lisi, S. Sarkar, and F. L. Villante, Phys. Rev. D **59**, 123520 (1999); K. A. Olive and D. Thomas, Astropart. Phys. **11**, 403 (1999).
[9] S. Burles and D. Tytler, Astrophys. J. **499**, 699 (1998); S. Burles and D. Tytler, Astrophys. J. **507**, 732 (1998); S. A. Levshakov, M. Dessauges-Zavadsky, S. D'Odorico, and P. Molaro (2001), astro-ph/0105529; J. M. O'Meara, D. Tytler, D. Kirkman, N. Suzuki, J. X. Prochaska, and A. M. Wolfe, Astrophys. J. **552**, 718 (2001); M. Pettini and D. V. Bowen, to appear in Astrophys. J. **560** (2001), astro-ph/0104474.
[10] K. A. Olive, E. D. Skillman, and G. Steigman, Astrophys. J. **483**, 788 (1997).
[11] Y. I. Izotov and T. X. Thuan, Astrophys. J. **500**, 188 (1998).
[12] R. Gruenwald, G. Steigman, and S. M. Viegas (2001), astro-ph/0109071; G. Stasińska and Y. I. Izotov (2001), astro-ph/0109253.
[13] J. C. Mather, et al., Astrophys. J. **512**, 511 (1999).

[14] K. A. Olive, D. N. Schramm, D. Thomas and T. P. Walker, Phys. Lett. B **265**, 239 (1991); H.-S. Kang and G. Steigman, Nucl. Phys. B **372**, 494 (1992).

[15] J. P. Kneller, R. J. Scherrer, G. Steigman, and T. P. Walker, Phys. Rev. D **64**, 123506 (2001).

[16] M. Tegmark, in *Proc. Enrico Fermi Summer School* (Varenna, 1995), Course CXXXII.

[17] X. Wang, M. Tegmark, and M. Zaldarriaga (2001), astro-ph/0105091.

[18] P. de Bernardis, et al., Nature **404**, 955 (2000); C. B. Netterfield, et al. (2001), astro-ph/0104460.

[19] A. Balbi, et al., Astrophys. J. Lett. **545**, L1 (2000); A. T. Lee, et al. (2001), astro-ph/0104459.

[20] N. W. Halverson, et al. (2001), astro-ph/0104489; C. Pryke, N. W. Halverson, E. M. Leitch, J. Kovac, J. E. Carlstrom, W. L. Holzapfel, and M. Dragovan (2001), astro-ph/0104490.

[21] S. Hannestad, Phys. Rev. D **64**, 083002 (2001).

[22] G. Mangano, A. Melchiorri, and O. Pisanti, Nucl. Phys. Proc. Suppl. **100** , 369 (2001); S. H. Hansen, G. Mangano, A. Melchiorri, G. Miele, and O. Pisanti, astro-ph/0105385.

[23] A. Sandage, Astrophys. J. **133**, 355 (1961).

[24] A. Goobar and S. Perlmutter, Astrophys. J. **450**, 14 (1995).

[25] S. Perlmutter, et al., Astrophys. J. **483**, 565 (1997); S. Perlmutter, et al., Astrophys. J. **517**, 565 (1999).

[26] A. G. Riess, et al., Astron. J. **114**, 722 (1997); A. G. Riess, et al., Astron. J. **116**, 1009 (1998); B. P. Schmidt, et al., Astrophys. J. **507**, 46 (1998).

[27] A. H. Jaffe, et al., Phys. Rev. Lett. **86**, 3475 (2001).

[28] B. Chaboyer, Phys. Rept. **307**, 23 (1998); R. Cayrel, et al., Nature **409**, 691 (2001); J. W. Truran, S. Burles, J. J. Cowan and C. Sneden, in *Astrophysical Ages and Time Scales, ASP Conference Series*, edited by T. von Hippel, N. Manset, and C. Simpson (2001), astro-ph/0109526.

[29] M. S. Turner, G. Steigman, and L. M. Krauss, Phys. Rev. Lett. **52**, 2090 (1984).

[30] G. Steigman and M. S. Turner, Nucl. Phys. B **253**, 375 (1985).

[31] J. M. Bardeen, J. R. Bond, and G. Efstathiou, Astrophys. J. **321**, 28 (1987); J. R. Bond and G. Efstathiou, Phys. Lett. B **265**, 245 (1991); M. White, G. Gelmini, and J. Silk, Phys. Rev. D **51**, 2669 (1995).

[32] S. J. McNally and J. A. Peacock, Mon. Not. R. Astron. Soc. **277**, 143 (1996); S. Bharadwaj and S. Sethi, Astrophys. J. Suppl. Ser. **114**, 37 (1998).

[33] M. S. Turner and M. White, Phys. Rev. D **56**, R4439 (1997).

[34] C. M. Baugh and G. Efstathiou, Mon. Not. R. Astron. Soc. **267**, 32 (1994); H. A. Feldman, N. Kaiser, and J. A. Peacock, Astrophys. J. **426**, 23 (1994); H. Lin, et al., Astrophys. J. **471**, 617 (1996).

[35] J. M. Bardeen, J. R. Bond, N. Kaiser, and A. S. Szalay, Astrophys. J. **304**, 15 (1986).

[36] N. Sugiyama, Astrophys. J. Suppl. Ser. **100**, 281 (1995).

[37] K. B. Fisher, C. A. Sharf, and O. Lahav, Mon. Not. R. Astron. Soc. **266**, 219 (1994); J. A. Peacock and S. J. Dodds, Mon. Not. R. Astron. Soc. **267**, 1020 (1994); M. Webster, S. L. Bridle, M. P. Hobson, A. N. Lasenby, O. Lahav, and G. Rocha, Astrophys. J. Lett. **509**, L65 (1998); D. Eisenstein and M. Zaldarriaga, Astrophys. J. **546**, 2 (2001).

[38] G. Efstathiou and S. J. Moody, Mon. Not. R. Astron. Soc. **325**, 1603 (2001).

[39] C. L. Bennett, et al., Astrophys. J. Lett. **464**, L1 (1994).

[40] E. F. Bunn, A. R. Liddle, and M. White, Phys. Rev. D **54**, 5917R (1996); E. F. Bunn and M. White, Astrophys. J. **480**, 6 (1997).

[41] Y. P. Jing, H. J. Mo, and G. Börner, Astrophys. J. **494**, 1 (1998); I. Zehavi, et al. (2001), astro-ph/0106476.

[42] G. G. Raffelt, *Stars as Laboratories for Fundamental Physics* (University of Chicago Press, Chicago, 1996).

[43] S. Hannestad, Phys. Rev. D **59**, 125020 (1999); M. Kaplinghat, R. E. Lopez, S. Dodelson, and R. J. Scherrer, Phys. Rev. D **60**, 123508 (1999); R. E. Lopez, S. Dodelson, R. J. Scherrer, and M. S. Turner, Phys. Rev. Lett. **81**, 3075 (1999).